Topological transitions of gapless paired states in mixed-geometry lattices

Dong-Hee Kim, Joel S. J. Lehikoinen, and Päivi Törmä*
COMP Centre of Excellence, Department of Applied Physics, Aalto University, FI-00076 Aalto, Finland

Fermion pairing may coexist with magnetism in unconventional superconductors and nuclear matter, stabilized by non-BCS mechanisms. Remarkable scenarios of exotic pairing with Fermi surfaces mismatched by chemical potential or mass difference have been suggested [1–4], inspiring experiments in solid-state materials [5, 6] and ultracold Fermi gases [7–10]. Here we propose fermionic species to be confined in lattices of *different geometry* and show how such distortion of symmetry leads to unconventional quantum states. In particular, we consider pairing of one species in a graphene-like lattice with another in a triangular sublattice. We find a rich phase diagram of multiband pairing with gapped and gapless excitations at zero temperature, implying that gapless superfluids can be stabilized in these systems. Quantum phase transitions between topologically distinct phases are predicted. Realization of mixed-geometry systems, e.g. using spin-dependent optical lattices [11–15], provides a new dimension to the ultracold quantum simulator for exploring unconventional quantum states of matter.

The standard BCS theory considers a perfectly symmetric pairing in up- and down-spin particles with opposite momenta lying on identical noninteracting Fermi surfaces. One of the fundamental issues in condensed matter physics is what would happen if this setting was broken, for instance, with mismatched Fermi surfaces between the two spin components. The Fulde-Ferrell–Larkin-Ovchinnikov (FFLO) state suggests Cooper pairs carrying finite center-of-mass momentum, causing a spatially oscillating order parameter [1, 2]. The Sarma or breached-pair (BP) state describes polarized superfluid of BCS-type zero-momentum pairs separated from unpaired excess particles forming a Fermi sea [3, 4]. These scenarios remain elusive but inspiring as possible unconventional pairing mechanisms.

Ultracold Fermi gases are potentially an ideal testbed of quantum many-body physics because of their unprecedented controllability [16]. Loaded in optical lattices, fermionic atoms with tunable interparticle interaction can construct the repulsive or attractive Hubbard model [17, 18]. One remarkable feature of ultracold gases is the tunability of asymmetry between the (pseudo-)spins associated with atomic internal states. Typical forms of spin asymmetry are population [7–10] or mass [19–21] imbalance between the spin components, or spin-dependent optical lattices realized for bosons [11–15]. The effects of anisotropic hopping or onsite potentials in a lattice [22, 23], as well as mixed-dimensional pairing in continuum [24, 25], have been theoretically investigated. Here we propose a fundamentally different type of asymmetry: a spin-dependent lattice where each spin component is separately loaded on a different underlying geometrical setup.

We propose a mixed-geometry setup of a two component Fermi gas where up- and down-spin components are loaded on honeycomb and triangular lattices, respectively, as shown in Fig. 1**a**. We argue that this is one of the simplest yet nontrivial mixed-geometry configurations. It is a superlattice of two spin-dependent sublattices A and B. Tuned on short-ranged interactions, this configuration can realize the Hubbard model with the onsite interaction selectively applied at A sites. The setup could be experimentally approached by generalizing the techniques in [11–15] or using two different atomic species [19–21].

We consider the attractive Hubbard model for a fermion pairing problem in the mixed-geometry lattices. As described in Methods, the mean-field Hamiltonian can be written in momentum space as

$$\mathcal{H}_{\mathrm{MF}} = \sum_{\vec{k}} \sum_{\alpha\in\{1,2,3\}} \xi_\alpha(\vec{k}) \hat{c}^\dagger_{\alpha\vec{k}} \hat{c}_{\alpha\vec{k}} + \sum_{\vec{k}} [g_1(\vec{k}) \hat{c}^\dagger_{1\vec{k}} \hat{c}^\dagger_{3,-\vec{k}} + g_2(\vec{k}) \hat{c}^\dagger_{2\vec{k}} \hat{c}^\dagger_{3,-\vec{k}} + \mathrm{h.c.}] \,, \tag{1}$$

which reveals a multiband system where up-spin particles in band $\alpha = 1, 2$ would pair with down-spin particles in band $\alpha = 3$. The lattice effects of the mixed geometry are encoded in the noninteracting band dispersion $\xi_\alpha(\vec{k})$ sketched in Fig. 1**b** and in the coupling $g_{1,2}(\vec{k})$. With fixed interaction and hopping strengths, two control parameters can govern the pairing in this system: 1) tuning chemical potentials can lead to the Fermi surface mismatch; 2) the onsite energy modulation $\tilde{\epsilon}$ controls a relative strength of the couplings g_1 and g_2.

Figure 1**d** shows the zero-temperature phase diagram for the case of the graphene-like up-spin bands ($\tilde{\epsilon} = 0$). We find that the diagram is divided into three main areas indicating the normal, gapped, and gapless phases. While the normal phase is simply indicated by a vanishing order parameter $\Delta = 0$, a paired state with nonzero Δ is discriminated by its single-particle excitation spectrum to be in the gapped or gapless phases. The gapped phase is a fully paired state, similar to the BCS state. In the gapless phases, we find an exotic paired state which we call the incomplete-breached-pair (iBP) state because of a partial breach found in momentum distribution.

Intriguingly, the iBP state can be further divided into

different subclasses by the topological arrangement of one or two Fermi surfaces, leading to Lifshitz transitions [26]. The iBP states undergo two types of transitions where the Fermi surface is either vanishing (2-FS to 1-FS) or transforming to a topologically different surface (Γ-centered to K-centered). In this mixed-geometry system, while the former is a continuous transition, it turns out that the latter can be continuous or discontinuous transitions which meet at a multicritical point (see Figs. 1**a**,2**a**). This end point of the discontinuous transition may be explained as the marginal quantum critical point of a Lifshitz transition in a two-dimensional interacting system [27].

The nature of the iBP states can be characterized by momentum distributions $n_{\uparrow,\downarrow}(\vec{k})$ and a momentum-resolved order parameter Δ_k shown in Fig. 2. While the jumps in $n_{\uparrow,\downarrow}(\vec{k})$ and Δ_k indicate the presence of the Fermi surfaces, the breach surrounded by these discontinuities shows clear contrast to that of the conventional BP state in momentum space. It turns out that the momentum-space breach in our iBP state shows a mixture of paired particles with finite Δ_k coexisting with unpaired excess majority species, rather than a perfect phase separation suggested by the conventional BP state. However, the Luttinger's theorem still holds for a conserved quantity (here $n_\uparrow - n_\downarrow$) in the broken symmetry phase [28], explaining the plateau of $n_\uparrow - n_\downarrow = 1$ observed between the Fermi surfaces.

Controlled by chemical potentials or densities, topologically different iBP states arise with distinct Fermi surface topologies. It is not only that the number of the Fermi surfaces essentially changes between one and two as observed for instance at $\mu_\uparrow = 0$, but also the shape of the Fermi surface undergoes a topological transition. Figure 2 shows the topologically different Fermi surfaces found in this system and the phase diagram of the corresponding distinct iBP states. Note that the transitions in our phase diagram are driven by densities or chemical potentials, which is in contrast to the BEC-BCS crossover for imbalanced two-component gases where the transition into the BP state with one Fermi surface may occur in the BEC regime driven by interaction [29, 30]. In addition, compared with a noninteracting case where a topological change of the Fermi surface occurs simply at the van Hove singularity at $|\mu| = 1$ (see Fig. 1**c**), it is notable that the transition lines in the interacting system are very different from $|\mu| = 1$ as indicated by our diagram of the phases with Γ- and K-centered Fermi surfaces.

The characteristics of the gapless phase can be also tuned by onsite energy modulation $\tilde{\epsilon}$. The effects of finite $\tilde{\epsilon}$ are two-fold. First, it opens a band gap in the noninteracting up-spin bands. Second, it creates an imbalance between the interband couplings g_1 and g_2 (see Eq. (1)) as described in Methods. Consequently, for a large negative $\tilde{\epsilon}$ giving $g_2 \gg g_1$, the contribution of the up-spin upper band ($\alpha = 1$) to the pairing can be significantly suppressed. Figure 3 displays the phase diagrams for $\tilde{\epsilon} = -1.0, -1.4, -1.8$, indicating that the gapless phase becomes less robust as $|\tilde{\epsilon}|$ increases. This apparent connection between the coupling imbalance and the stability of the gapless phase implies that a well-balanced interband contribution may be an important factor for our mixed-geometry lattice in stabilizing the iBP phase.

One of the main findings is the chemical-potential-driven emergence of the paired states with zero, one, and two Fermi surfaces. The importance of the multiband contribution to the formation of these exotic paired states can be intuitively understood in the band structure of the mixed-geometry system. Revisiting our mean-field procedures (see Methods), as illustrated in Fig. 4, there are three cases of zero, one, and two crossings allowed between the noninteracting particle-like ($\xi_\uparrow$) and hole-like ($-\xi_\downarrow$) dispersions with varying chemical potentials. The interaction ($g_{1,2}$) causes band repulsion and gaps at crossings, leading to the two different configurations of quasiparticle energy dispersions. Depending on the chemical potentials, the zero excitation level indicates the formation of zero, one, or two Fermi surfaces (see Fig. 4**b**).

The simple band picture can also clarify the arrangements of the distinct iBP states in the phase diagrams. For instance, considering the iBP state with two Fermi surfaces, Fig. 4**b** indicates that there are two multiband configurations forming such states, the one in the lower band side (**d**) and the other in the upper band side (**f**). In contrast, the state with one Fermi surface occurs only in the upper band side (**e**). This classification in the band picture is consistent with the phase boundaries in the phase diagrams. In addition, the band picture indicates that the iBP states with two Fermi surfaces have a different nature depending on whether they originate from the upper or lower band side. Indeed, for instance, the momentum distributions found at $\tilde{\epsilon} = -1.8$ show a fully polarized normal area of excess majority particles around K, which is in contrast to the fully paired area around K observed in its counterpart found at $\tilde{\epsilon} = 0$ (see Fig. 3**c**). Systematic study of finite temperature effects and quantum fluctuations is beyond the scope of this work. While the Fermi surface is strictly defined at zero temperature, we have tested that the main features are present at finite temperatures within the mean-field theory, critical temperatures being typically of the order of a tenth of the hopping amplitude.

Mixed-geometry lattice systems as we propose here extend the realm of pairing and strong correlation physics. The attractive Hubbard model in the mixed honeycomb-triangular lattice that we have considered reveals a new exotic multiband paired state, the incomplete-breached-pair state, and shows a rich phase diagram of topologically distinct phases. We have found that multiband pairing plays a key role in stabilizing the coexistence of pairing and magnetization, which may have an interest-

ing connection to multiband effects and magnetic fluctuations interplaying in solid-state superconductors such as iron-based materials and MgB_2. We argue that realizing mixed-geometry lattices would open a new dimension to the search for novel quantum states with ultracold gases as quantum simulators.

METHODS

Attractive Hubbard model. The Hubbard Hamiltonian in the mixed-geometry lattice system considered becomes

$$\begin{aligned}\mathcal{H} = &- t_\uparrow \sum_{\langle i,j\rangle\in\mathcal{L}_\uparrow} (\hat{a}^\dagger_{i\uparrow}\hat{b}_{j\uparrow} + h.c.) + \epsilon^a_\uparrow \sum_i \hat{n}^a_{i\uparrow} + \epsilon^b_\uparrow \sum_i \hat{n}^b_{i\uparrow} \\ &- t_\downarrow \sum_{\langle i,j\rangle\in\mathcal{L}_\downarrow} (\hat{a}^\dagger_{i\downarrow}\hat{a}_{j\downarrow} + h.c.) + \epsilon^a_\downarrow \sum_i \hat{n}^a_{i\downarrow} \\ &- \mu_\uparrow \sum_{i,j} (\hat{n}^a_{i\uparrow} + \hat{n}^b_{j\uparrow}) - \mu_\downarrow \sum_i \hat{n}^a_{i\downarrow} - U \sum_i \hat{n}^a_{i\uparrow}\hat{n}^a_{i\downarrow} \ ,\end{aligned}$$

where $\hat{a}^\dagger$ ($\hat{a}$) and $\hat{b}^\dagger$ ($\hat{b}$) are fermionic creation (annihilation) operators in the sublattices A and B, respectively, and the density operators $\hat{n}^a$ and $\hat{n}^b$ denote $\hat{a}^\dagger\hat{a}$ and $\hat{b}^\dagger\hat{b}$. The spin-dependent hopping occurs between nearest-neighboring sites $\langle i,j\rangle$ in the up-spin honeycomb lattice $\mathcal{L}_\uparrow$ and the down-spin triangular lattice $\mathcal{L}_\downarrow$, while the hopping strengths $t_\uparrow$ and $t_\downarrow$ are set to be unity for simplicity. Introducing the control parameter $\tilde{\epsilon}$ for onsite energy modulations, the onsite terms are chosen as $\epsilon^a_\uparrow = \tilde{\epsilon}/2$ $\epsilon^b_\uparrow = -\tilde{\epsilon}/2$, and $\epsilon^a_\downarrow = -3$ without loss of generality since other possible tunings of onsite energies can be absorbed into the spin-dependent chemical potentials $\mu_\uparrow$ and $\mu_\downarrow$. The onsite interaction is chosen as $U = 5$.

Mean-field theory. The mean-field order parameter is defined as $\Delta = U\langle\hat{a}_{i\downarrow}\hat{a}_{i\uparrow}\rangle$. Neglecting fluctuations, the interaction term can be approximated as $-U\sum_i \hat{n}^a_{i\uparrow}\hat{n}^a_{i\downarrow} \approx -\sum_i(\Delta\hat{a}^\dagger_{i\uparrow}\hat{a}^\dagger_{i\downarrow} + \Delta^*\hat{a}_{i\downarrow}\hat{a}_{i\uparrow}) + |\Delta|^2/U$. Possible Hartree shifts can be incorporated into the chemical potentials and the onsite energy modulation $\tilde{\epsilon}$. Performing the Fourier transformation, $\tilde{f}_{\vec{k}\sigma} = \sum_i e^{-i\vec{k}\cdot\vec{x}_i}\hat{f}_{i\sigma}$ where f is a or b, the noninteracting part of the Hamiltonian can be written in the basis of $\tilde{\Phi}^\dagger_{\vec{k}} \equiv (\tilde{a}^\dagger_{\vec{k}\uparrow}, \tilde{b}^\dagger_{\vec{k}\uparrow}, \tilde{a}^\dagger_{\vec{k}\downarrow})$ as $\mathcal{H}^0 = \sum_{\vec{k}} \tilde{\Phi}^\dagger_{\vec{k}}\mathbf{H}^{(0)}_{\vec{k}}\tilde{\Phi}_{\vec{k}}$ with the matrix representation

$$\mathbf{H}^{(0)}_{\vec{k}} = \begin{pmatrix} \tilde{\epsilon} - \mu_\uparrow & h_\uparrow(\vec{k}) & 0 \\ h^*_\uparrow(\vec{k}) & -\tilde{\epsilon} - \mu_\uparrow & 0 \\ 0 & 0 & \xi_\downarrow(\vec{k}) \end{pmatrix},$$

where $h_\uparrow(\vec{k}) = -t_\uparrow[e^{\frac{ik_x}{\sqrt{3}}} + 2e^{\frac{-ik_x}{2\sqrt{3}}}\cos\frac{k_y}{2}]$ and $\xi_\downarrow(\vec{k}) = -t_\downarrow[\cos k_y + \cos\frac{1}{2}(k_y + \sqrt{3}k_x) + \cos\frac{1}{2}(k_y - \sqrt{3}k_x) - 3] - \mu_\downarrow$. Accordingly, the order parameter can be rewritten with the momentum resolution as $\Delta \equiv \sum_{\vec{k}}\Delta_{\vec{k}} = U\sum_{\vec{k}}\langle\hat{a}_{-\vec{k}\downarrow}\hat{a}_{\vec{k}\uparrow}\rangle$. We see that, in momentum space, the up-spin particles at different sites (A or B) are coupled. A more natural form of the noninteracting Hamiltonian is obtained by choosing a new basis set that diagonalizes $\mathbf{H}^{(0)}_{\vec{k}}$. The transformed fermionic operators $\hat{c}^\dagger_{\alpha\vec{k}}$ and $\hat{c}_{\alpha\vec{k}}$ with the index $\alpha \in \{1,2,3\}$ then represent the noninteracting energy bands $\xi_\alpha(\vec{k})$, where 1 and 2 denote the upper and lower bands of the up-spin component, and 3 indicates the down-spin band. In the basis $\tilde{\Psi}^\dagger_{\vec{k}} \equiv (\hat{c}^\dagger_{1\vec{k}}, \hat{c}^\dagger_{2\vec{k}}, \hat{c}_{3-\vec{k}})$, the full mean-field Hamiltonian is rewritten as $\mathcal{H}_{\rm MF} = \sum_{\vec{k}}\tilde{\Psi}^\dagger_{\vec{k}}\mathbf{H}_{\vec{k}}\tilde{\Psi}_{\vec{k}} + \sum_{\vec{k}}\xi_3(-\vec{k}) + |\Delta|^2/U$ with the matrix representation

$$\mathbf{H}_{\vec{k}} = \begin{pmatrix} \xi_1(\vec{k}) & 0 & g^*_1(\vec{k}) \\ 0 & \xi_2(\vec{k}) & g^*_2(\vec{k}) \\ g_1(\vec{k}) & g_2(\vec{k}) & -\xi_3(-\vec{k}) \end{pmatrix}, \qquad (2)$$

where the diagonal terms are the noninteracting band dispersions $\xi_{1,2}(\vec{k}) = \pm\sqrt{\tilde{\epsilon}^2 + |h_\uparrow(\vec{k})|^2} - \mu_\uparrow$ and $\xi_3(\vec{k}) = \xi_\downarrow(\vec{k})$, and the interband couplings are derived as

$$g_{1,2}(\vec{k}) = -\frac{\Delta}{\sqrt{2}}\left[1 \pm \frac{\tilde{\epsilon}}{\sqrt{\tilde{\epsilon}^2 + |h_\uparrow(\vec{k})|^2}}\right]^{\frac{1}{2}}.$$

This gives the Hamiltonian of Eq. 1. The quasiparticle energies $E_\alpha(\vec{k})$ where $\alpha \in \{1,2,3\}$ can be obtained by diagonalizing $\mathbf{H}_{\vec{k}}$, and from the grand partition function $\mathcal{Z} = \mathrm{Tr}\exp[-\beta\mathcal{H}_{\rm MF}]$, the grand potential $\Omega \equiv -\frac{1}{\beta}\ln\mathcal{Z}$ is calculated as

$$\Omega(\Delta) = \frac{|\Delta|^2}{U} + \sum_{\vec{k}}\xi_3(-\vec{k}) + \frac{1}{\beta}\sum_{\vec{k},\alpha}\ln(1 + e^{-\beta E_\alpha(\vec{k})}).$$

The ground state is self-consistently obtained by the order parameter Δ minimizing the grand potential Ω, which in principle is equivalent to solving a gap equation but finds only stable solutions.

* paivi.torma@aalto.fi

[1] Fulde, P. & Ferrell, R. A. Superconductivity in a strong spin-exchange field. *Phys. Rev.* **135**, A550–A563 (1964).

[2] Larkin, A. I. & Ovchinnikov, Y. N. Inhomogeneous state of superconductors. *Sov. Phys. JETP* **20**, 762–769 (1965).

[3] Sarma, G. On the influence of a uniform exchange field acting on the spins of the conduction electrons in a superconductor. *J. Phys. Chem. Solids* **24**, 1029–1032 (1963).

[4] Liu, W. V. & Wilczek, F. Interior gap superfluidity. *Phys. Rev. Lett.* **90**, 047002 (2003).

[5] Radovan, H. *et al.* Magnetic enhancement of superconductivity from electron spin domains. *Nature* **425**, 51–55 (2003).

[6] Kenzelmann, M. *et al.* Coupled superconducting and magnetic order in $CeCoIn_5$. *Science* **321**, 1652–1654 (2008).

[7] Zwierlein, M. W., Schirotzek, A., Schunck, C. H. & Ketterle, W. Fermionic superfluidity with imbalanced spin populations. *Science* **311**, 492–496 (2006).

[8] Partridge, G. B., Li, W., Kamar, R. I., Liao, Y. & Hulet, R. G. Pairing and phase separation in a polarized Fermi gas. *Science* **311**, 503–505 (2006).

[9] Nascimbéne, S. *et al.* Collective oscillations of an imbalanced Fermi gas: axial compression modes and polar on effective mass. *Phys. Rev. Lett.* **103**, 170402 (2009).

[10] Liao, Y. *et al.* Spin-imbalance in a one-dimensional Fermi gas. *Nature* **467**, 567–569 (2010).

[11] LeBlanc, L. J. & Thywissen, J. H. Species-specific optical lattices. *Phys. Rev. A* **75**, 053612 (2007).

[12] Catani, J. *et al.* Entropy exchange in a mixture of ultracold atoms. *Phys. Rev. Lett.* **103**, 140401 (2009).

[13] Lamporesi, G. *et al.* Scattering in mixed dimensions with ultracold gases. *Phys. Rev. Lett.* **104**, 153202 (2010).

[14] Soltan-Panahi, P. et al. Multi-component quantum gases in spin-dependent hexagonal lattices. *Nature Phys.* **7**, 434–440 (2011).

[15] Soltan-Panahi, P., Lühmann, D.-S., Struck, J., Windpassinger, P. & Sengstock, K. Quantum phase transition to unconventional multi-orbital superfluidity in optical lattices. *Nature Phys.* **8**, 71–75 (2012).

[16] Bloch, I., Dalibard, J. & Zwerger, W. Many-body physics with ultracold gases. *Rev. Mod. Phys.* **80**, 885–964 (2008).

[17] Jördens, R., Strohmaier, N., Günter, K., Moritz, H. & Esslinger, T. A Mott insulator of fermionic atoms in an optical lattice. *Nature* **455**, 204–207 (2008).

[18] Schneider, U. *et al.* Metallic and insulating phases of repulsively interacting fermions in a 3D optical lattice. *Science* **322**, 1520–1525 (2008).

[19] Wille, E. *et al.* Exploring an ultracold Fermi-Fermi mixture: interspecies Feshbach resonances and scattering properties of ^{6}Li and ^{40}K. *Phys. Rev. Lett.* **100**, 053201 (2008).

[20] Voigt, A.-C. *et al.* Ultracold heteronuclear Fermi-Fermi molecules. *Phys. Rev. Lett.* **102**, 020405 (2009).

[21] Kohstall, C. *et al.* Metastability and coherence of repulsive polarons in a strongly interacting Fermi mixture. *Nature* **485**, 615–618 (2012).

[22] Feiguin, A. E. & Fisher, P. A. Exotic paired states with anisotropic spin-dependent Fermi surfaces. *Phys. Rev. Lett.* **103**, 025303 (2009).

[23] Zapata, I., Wunsch, B., Zinner, N. T. & Demler, E. π phases in balanced fermionic superfluid on spin-dependent optical lattices. *Phys. Rev. Lett.* **105**, 095301 (2010).

[24] Nishida, Y. & Tan, S. Universal Fermi gases in mixed dimensions. *Phys. Rev. Lett.* **101**, 170401 (2008).

[25] Iskin, M. & Subaşi, A. L. Cooper pairing and BCS-BEC evolution in mixed-dimensional Fermi gases. *Phys. Rev. A* **82**, 063628 (2010).

[26] Lifshitz, I. M. Anomalies of electron characteristics of a metal in the high pressure region. *Sov. Phys. JETP* **11**, 1130–1135 (1960).

[27] Yamaji, Y., Misawa, T. & Imada, M. Quantum and topological criticalities of Lifshitz transition in two-dimensional correlated electron systems. *J. Phys. Soc. Jpn* **75**, 094719 (2006).

[28] Sachdev, S. & Yang, K. Fermi surfaces and Luttinger's theorem in paired fermion systems. *Phys. Rev. B* **73**, 174504 (2006).

[29] Pao, C.-H., Wu, S.-T. & Yip, S.-K. Superfluid stability in the BEC-BCS crossover. *Phys. Rev. B* **73**, 132506 (2006).

[30] Sheehy, D. E. & Radzihovsky, L. BEC-BCS crossover in "magnetized" Feshbach-resonantly paired superfluids. *Phys. Rev. Lett.* **96**, 060401 (2006).

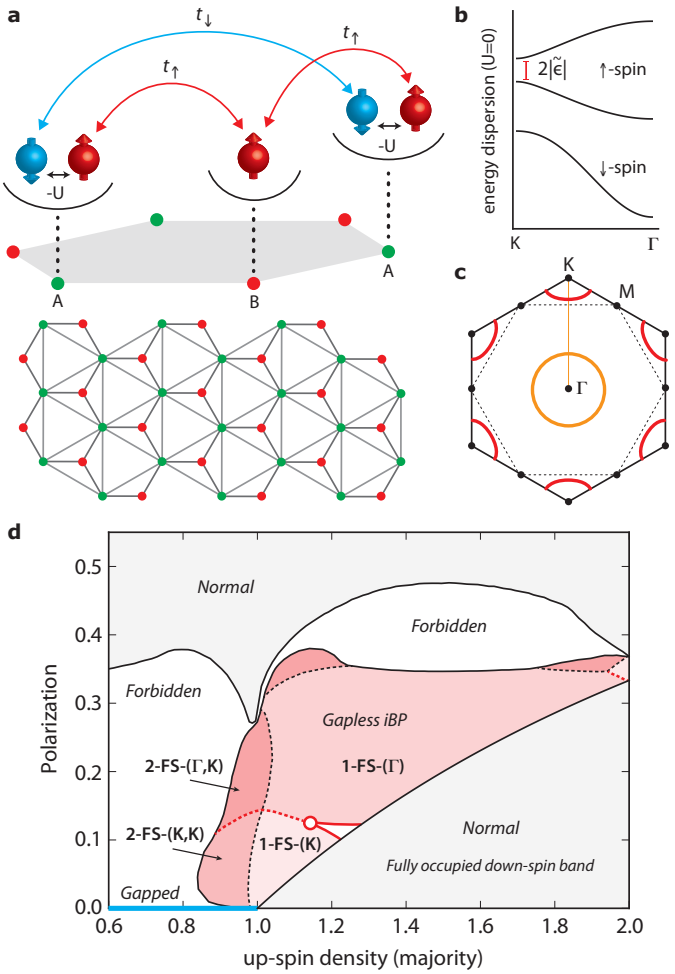

FIG. 1. **The mixed-geometry lattice proposed and the phase diagram of exotic paired states at zero temperature. a**. Up-spin and down-spin components are selectively loaded on honeycomb (up-spin, sublattices A and B) and triangular (down-spin, sublattice A) lattices. The attractive Hubbard model is considered in the mixed-geometry lattice. Noninteracting band dispersions are sketched in **b**, where the gap in up-spin bands is tuned by the onsite energy modulation $\tilde{\epsilon}$ (see Methods). **c**. The Γ-centered and K-centered Fermi surfaces are sketched. The high symmetry points Γ, K, and M are indicated in the first Brillouin zone. In a noninteracting system, a transition between the Γ- and K-centered shapes occurs at the van Hove singularity at $|\mu| = 1$ where the Fermi surface is a hexagon (dotted line). **d**. The phase diagram is plotted as a function of up-spin density $n_\uparrow$ and polarization $P = (n_\uparrow - n_\downarrow)/(n_\uparrow + n_\downarrow)$ for the case of $\tilde{\epsilon} = 0$. The gapped and gapless paired phases and the normal phase are identified. The gapless states are further characterized by the Fermi surface topology denoted as z-FS-(X) indicating z Fermi surfaces being centered at the high symmetry points (X). Continuous (dotted lines) and discontinuous (solid lines) Lifshitz transitions are found, and the empty circle indicates the multicritical point.

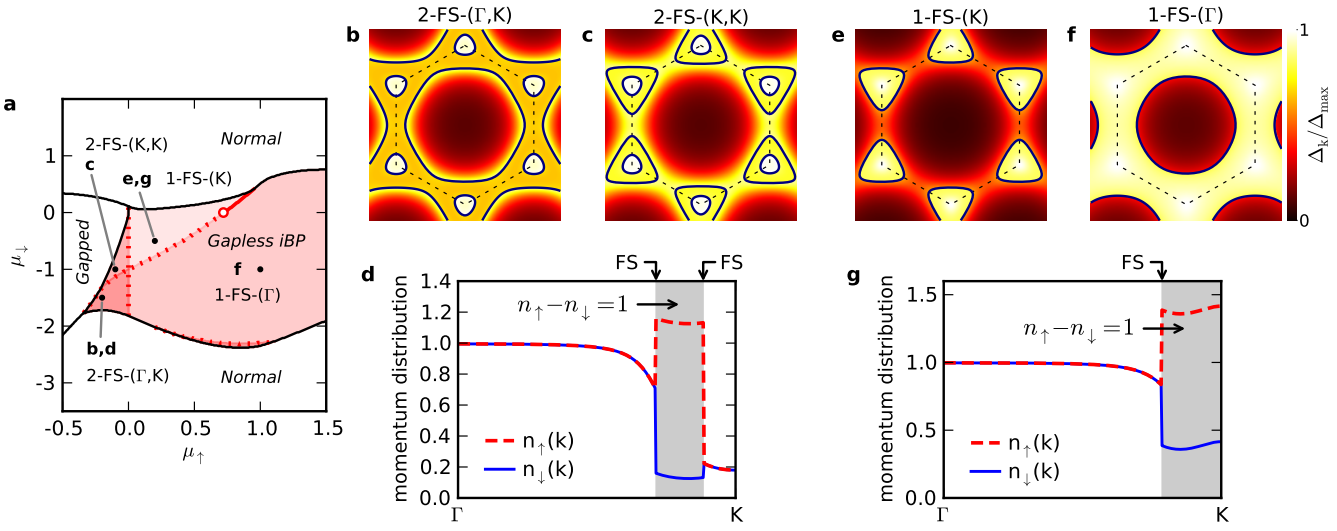

FIG. 2. **Characterization of paired states in the gapless phase.** Representative Fermi surface configurations are shown with momentum-resolved order parameter over the first Brillouin zone (dashed line) in **b**, **c**, **e**, and **f** sampled from topologically distinct states given in **a**. The phase diagram (**a**) is plotted as a function of the chemical potentials $\mu_\uparrow$ and $\mu_\downarrow$ for $\tilde{\epsilon} = 0$. The dotted and solid lines indicate continuous and discontinuous topological transitions which meet at the multicritical point indicated by the empty circle. The multicritical point corresponds to the fully filled down-spin band ($\mu_\downarrow = 0$) in a noninteracting system showing a step-function-like singularity in the density of states. Momentum distributions in **d** and **g** further characterize the gapless paired states found in this system with 2-FS and 1-FS. The existence of plateaus of $n_\uparrow - n_\downarrow$ in the shaded area enclosed by the Fermi surfaces is an indication of Luttinger's theorem. This mixed-geometry system shows pairing coexisting with polarization in momentum space in the gapless phase, in contrast to the phase separation in the usual breached-pair state.

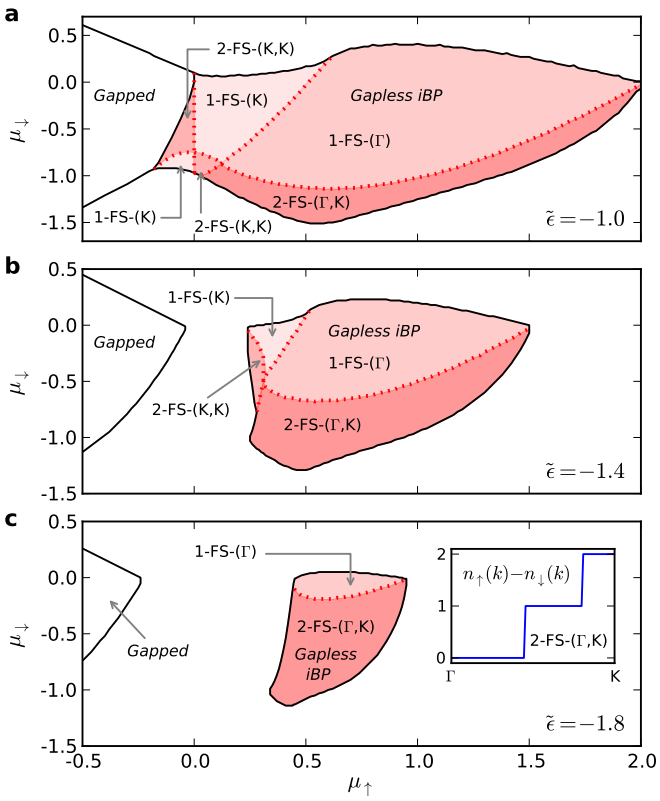

FIG. 3. **Effects of the onsite energy modulation.** The phase diagrams are examined for the onsite energy modulation $\tilde{\epsilon} = -1.0$ (**a**), -1.4 (**b**), and -1.8 (**c**). While the gapped phase is insensitive to $\tilde{\epsilon}$, the gapless phase (shaded) shows different Fermi surface topologies as $\tilde{\epsilon}$ changes. Compared with the phase diagram for $\tilde{\epsilon} = 0$ in Fig. 2**a**, while the 1-FS-(Γ) state is relatively robust, the areas of other incomplete-breached-pair states at $\tilde{\epsilon} = 0$ are largely changed. In particular, a dominant phase at a large $\tilde{\epsilon}$ is found to be the 2-FS-(Γ, K) state which turns out to be a different state from the one dominant at $\tilde{\epsilon} = 0$. This 2-FS-(Γ, K) state at finite ϵ corresponds to case **f** in Fig. 4**b** rather than case **d**, showing a different momentum distribution with a fully polarized area as schematically shown in the inset of **c**.

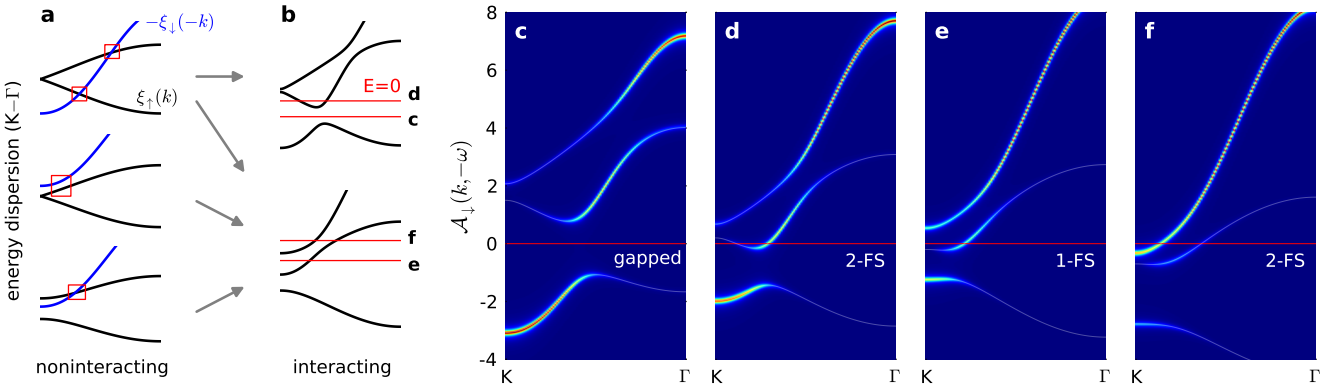

FIG. 4. **Schematics of pairing gap opening and Fermi surface formation.** The band dispersions and spectral functions are shown along the K−Γ line in the first Brillouin zone. **a**. The noninteracting particle-like up-spin bands ($\xi_\uparrow$) and the hole-like down-spin band (-$\xi_\downarrow$) are illustrated, possible points for level repulsion and gap formation are shown by empty boxes. **b**. The resulting quasiparticle bands with interaction turned on are sketched with possible locations of the zero excitation level ($E = 0$), showing the formation of zero (**c**), one (**e**), and two Fermi surfaces (**d**,**f**). The arrows indicate the possible evolutions from the noninteracting bands to the quasiparticle bands. The actual spectral functions of the down-spin component, $\mathcal{A}_\downarrow(k, -\omega)$, for all typical cases are selected for display in **c**-**f**.